Article

Numerical Modeling of the Dynamic Elastic Modulus of Concrete

Gustavo de Miranda Saleme Gidrão * and Ricardo Carrazedo

Posted Date: 18 April 2023

doi: 10.20944/preprints202304.0521.v1

Keywords: dynamical properties; dynamic elastic modulus; concrete; mortar; mixture parameters; acoustic test; composite theory

Article

Numerical Modeling of the Dynamic Elastic Modulus of Concrete

Gustavo de Miranda Saleme Gidrão [1,*], Ricardo Carrazedo [2], Rúbia Mara Bosse [1], Laura Silvestro [1], Rodrigo Ribeiro [1] and Carlos Francisco Pecapedra de Souza [1]

[1] Department of Civil Engineering, Federal University of Technology-Paraná (UTFPR), Guarapuava 85053-525, PR, Brazil

[2] School of Engineering of São Carlos, University of Sao Paulo, Av. Trabalhador Saocarlense, 400, Sao Carlos 13566-590, SP, Brazil

* Correspondence: gidrao@utfpr.edu.br

Abstract: This article introduces simulations of theoretical material with controlled properties for the evaluation of the effect of key parameters, as volumetric fractions, elastic properties of each phase and transition zone on the effective dynamic elastic modulus. The accuracy level of classical homogenization models was checked regarding the prediction of dynamic elastic modulus. Numerical simulations were performed with finite element method for evaluations of the natural frequencies and their correlation with E_d, through frequency equations. An acoustic test validated the numerical results and obtained the elastic modulus of concretes and mortars at 0.3, 0.5 and 0.7 water-cement ratios. Hirsch calibrated according to the numerical simulation (x = 0.27) exhibited a realistic behavior for concretes of w/c = 0.3 and 0.5, with 5% error. Nevertheless, for w/c = 0.7, Young Modulus approached Reuss model, similarly to theoretical triphasic materials. Hashin-Shtrikman bounds is not perfectly applied to theoretical biphasic materials under dynamic situations.

Keywords: dynamical properties; dynamic elastic modulus; concrete; mortar; mixture parameters; acoustic test; composite theory

1. Introduction

Dynamic modulus of elasticity (E_d) is related to a very small instantaneous strain, geometrically similar to the initial tangent modulus [1]. Mehta and Monteiro [1] reported E_d higher than the initial tangent modulus in approximately 20%, 30% and 40%, for concretes of high, medium and low resistance. Nevertheless, the relation between the static and dynamic moduli is not precise, since no physics law correlates their values to the necessary precision [1–3]. The use of E_d, which can be accurately determined by acoustic tests [4,5], is more appropriate for analyses of structures subjected to impact loading [1], e.g., vibration serviceability limit state.

E_d is strongly influenced by mixture parameters, such as water-cement ratio of mortar (porosity), maturity, elastic properties of coarse aggregate, volumetric fraction of interfacial transition zone (ITZ) and aggregate-cement proportion [1,3,6–8].

Classical models predict with success the elastic modulus of a perfect biphasic composite. Since 19th century, homogenization models, as Voigt (or parallel) [1,9–12] and Reuss [1,10–13] (or series) have been used for determining the elastic static properties of concretes. According to Hill [14], Voigt and Reuss are upper and lower bounds for any biphasic material. Hashin-Shtrikman (H-S) [11,15] developed the most stringent bounds of behavior for a composite material [11,15–17]. Nilsen and Monteiro [16,17] showed limitations in the application of H-S bounds, since concrete is not a perfectly biphasic material. Consequently, a third composite component (i.e., Transition Zone, ITZ) must be considered in the model. In 2013, Nemat-Nasser and Srivastava [18] reported another limitation of H-S bounds: the approach cannot apply to dynamic situations perfectly. This is a severe limitation, especially for the estimation of dynamic elastic modulus through modal analysis.

Other classical homogenization models have predicted the elastic properties of biphasic materials. Counto [1,11] assumed a prismatic coarse aggregate in the center of the mortar prism, whereas Hansen [1,11] adopted a spherical coarse aggregate in the same region. Hirsch [1,11] proposed a semi empirical model that relates the modulus of elasticity of the concrete to the Young modulus' of the two phases (aggregate and matrix), their volume fractions, and an empirical constant, x. The "x value" is a combination factor obtained by Voigt and Reuss models and calibrated either experimentally, or via a numerical simulation. Topçu [11] obtained x = 0.3 experimentally. The present study aims to obtain x through numerical simulations.

Sophisticated models have been proposed towards predictions of effects, as size and shape of aggregate particles and influence of porosity and transition zone [19–26]. Hashin and Monteiro [27] described concrete as a three-phase material formed by a matrix with embedded spherical particles and surrounded by a concentric spherical shell that represents an ITZ. According to the authors, the Young's modulus of ITZ is 50% of the elastic modulus of the cement mortar (i.e., $E_{ITZ} = E_m/2$). Duplan et al. [28] designed a very realistic model constituted by aggregates surrounded by a layer of ITZ and a layer of cement paste, while air bubbles are considered mono-sized inclusions with no elastic behavior, which result in 5% error. Zheng, Zhou and Jin [22,23] proposed a model in which concrete is represented as a three-phase composite material composed of mortar, spherical or elliptical aggregate and an inhomogeneous ITZ, based on semi-empirical gradient model, dependent on water/cement ratio, degree of hydration, and porosity at the ITZ. Pichler et al. [26] predict the dynamic modulus of cements pastes with w/c = 0.35 and 0.60, considering a material constituted by clinker, pores (with spherical shapes) and hydration products (with spherical and/or non-spherical shapes).

Although such models are complex for practical applications, those recent studies have opened up new possibilities for the micromechanical modeling of concrete through numerical simulations, especially simulations that allow the study of dynamic elastic modulus (E_d). The current research focuses on simulations of the concrete as a 2D theoretical material (biphasic or triphasic) with controlled elastic properties of each phase (mortar and aggregate). The purpose is to evaluate the behavior of dynamic effective elastic modulus (E_d) regarding porosity, individual elastic properties of coarse aggregate and/or mortar (i.e., E_a , ν_a, E_m and ν_m, respectively), volumetric fraction, and the presence of ITZ with known properties (i.e. ITZ thickness and elastic modulus E_{ITZ}). Further, this approach with controlled properties was compared with classical models, as Voigt, Reuss, Hirsch, H-S, Hansen and Counto, aiming show the most accuracy classical model could predict the E_d. An experimental validation showed the coherence and limitations of our numerical simulations. Therefore, this paper advances in the methodology to predict the dynamic elastic modulus of concrete and contributes to comprehension of its response under dynamical excitations.

2. Numerical simulations

Numerical simulations were performed with the general-purpose finite element software Abaqus release 6.14. A theoretical material was modeled by a 150 mm x 150 mm x 50 mm square with fined mesh 1 mm maximum dimension and a quadrilateral and four-node bilinear element with reduced integration (CPS4R, Figure 1.a). Plane stress was considered in this 2D shell structure. This model was chosen due the low computational cost. The boundary conditions weren't considered in the model, representing a free model subject to vibrations..

In this study, modal analysis in Abaqus with the Lanczos solution method was utilized to investigate the dynamic behavior of a free shell structure. The Lanczos solution is an iterative method that enables the calculation of the eigenvectors and eigenvalues of a large sparse symmetric matrix, making it ideal for modal analysis. The shell structure was modeled using a linear elastic material with a Poisson ratio and elastic modulus, and a density of 2400 kg/m^3 was considered. The shell was allowed to vibrate freely to demonstrate all modes of vibration. Abaqus was employed to generate the mass and rigidity matrices and to determine the eigenvalues and eigenvectors for the shell structure.

Preprints (www.preprints.org) | NOT PEER-REVIEWED | Posted: 18 April 2023 doi:10.20944/preprints202304.0521.v1

2.1. Frequency equations of an Isotropic and homogeneous material

The relation between 1st natural frequency (bending or shear mode of vibration) and Effective elastic properties are established. The theoretical modal analysis determines the shear and flexural 1st natural frequency for a free vibration of a homogeneous isotropic square structure (see Figure 1). "Shear" frequency can be related to Effective Dynamic Shear Modulus (G_d), whereas "flexural" frequency is associated with Effective Dynamic Elastic Modulus (E_d) [4,5,29] through "Frequency equations".

Table 1 shows an analysis performed with a homogeneous isotropic material of $\rho = 2400$ kg/m^3 density and variations in elastic and shear modulus. Simulations determined the frequency equation and confirmed the expected relationships of "shear" frequency and shear modulus (Eq. 1), as well as "bending" frequency and elastic modulus (Eq. 2), see Figure 2. Constants C_1 and C_2 are dependent on the geometry of the specimens and were determined by a linear regression analysis, $C_1 = 131.16$ and $C_2 = 87.56$ (with $R^2 \rightarrow 1$), respectively.

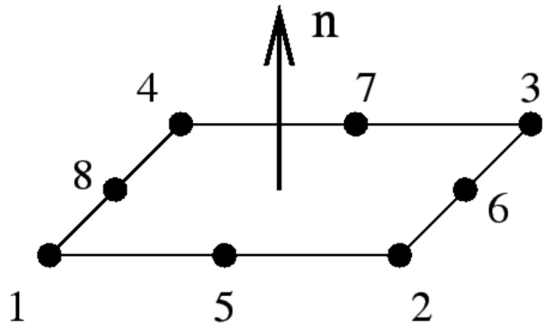

(a) CPS4R element

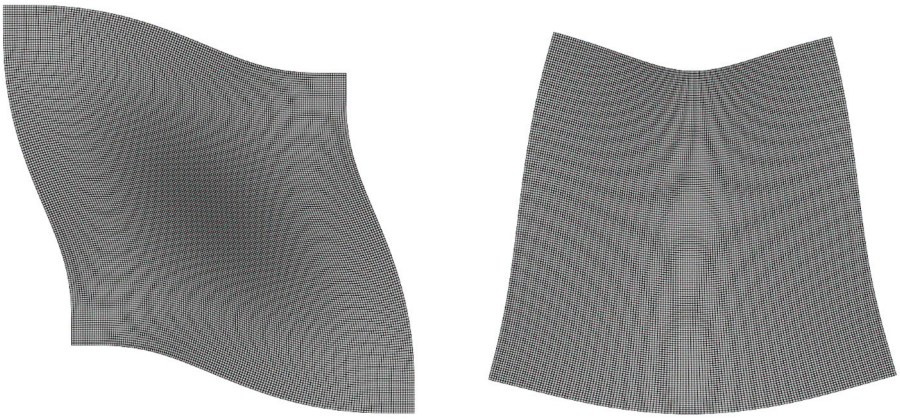

(b) "Shear" mode (c) "Bending" mode

Figure 1. Vibration modes considered in the numerical analysis.

$$f_{shear} = C_1 \sqrt{\frac{G_d}{\rho}} \quad (1)$$

$$f_{bend} = C_2 \sqrt{\frac{E_d}{\rho}} \quad (2)$$

Preprints (www.preprints.org) | NOT PEER-REVIEWED | Posted: 18 April 2023 doi:10.20944/preprints202304.0521.v1

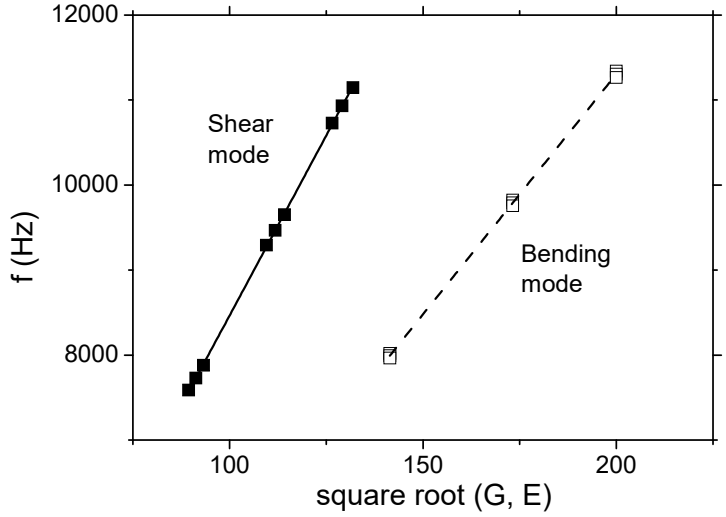

Figure 2. Vibration modes considered in the numerical analysis.

Table 1. Elastic parameters and corresponding frequencies.

E (MPa)		G (MPa)	$\sqrt{E}$	f_{bend} (Hz)	$\sqrt{G}$	f_{shear} (Hz)
20000	0.15	8696	141.4	8020	93.3	7881
20000	0.2	8333	141.4	7994	91.3	7730
20000	0.25	8000	141.4	7965	89.4	7587
30000	0.15	13043	173.2	9822	114.2	9652
30000	0.2	12500	173.2	9790	111.8	9467
30000	0.25	12000	173.2	9756	109.5	9292
40000	0.15	17391	200.0	11341	131.9	11145
40000	0.2	16667	200.0	11305	129.1	10931
40000	0.25	16000	200.0	11265	126.5	10729

2.2. Effect of Porosity

Influence of porosity (P) was checked on effective elastic properties G_d and E_d. We suppose a theoretical material constituted by spherical voids of 3 mm diameter, distributed in a matrix (e.g. Figure 3). Voids were incrementally added to the matrix, i.e., 4 voids (2 by 2 – 0.13 % porosity) until 1296 voids (36 by 36 – 40.72 % porosity). For all cases, the cement paste had constant properties of ρ_p = 2100 kg/m³, E_p = 20000 MPa and v_p = 0.2, whereas the voids had ρ_v = 1 kg/m³ and E_v = 0,1 MPa (i.e., ρ_v/ρ_p = 0.0004 and E_v/E_p = 0.000005). An approximately 0.13 % to 40.72% porosity increase decreased E_d (Figure 4), since porosity is inversely linked to the material rigidity [8]. Boccacini and Fan [30] reviewed several theoretical models to correlate E_d and porosity of ceramic materials. Hanselmann-Hashin [31,32] (Eq. 3) and Mackenzie [33] (Eq. 4) achieved the best fit with numerical results (see Figure 4 and Table 2). The fit with R^2 close to 0.97 showed coherence of simulations.

$$E = E_0\left(1+\frac{AP}{1-(A+1)P}\right) \quad (3)$$

$$E(P) = E_0[1-K\times P+(K-1)\times P^2] \quad (4)$$

where E is the effective elastic modulus, E_0 is the intact elastic modulus under porosity equal to zero (value recovered from $E_0 \cong 30000$ MPa), P is porosity and A and K are empirical adjustments;

Preprints (www.preprints.org) | NOT PEER-REVIEWED | Posted: 18 April 2023 doi:10.20944/preprints202304.0521.v1

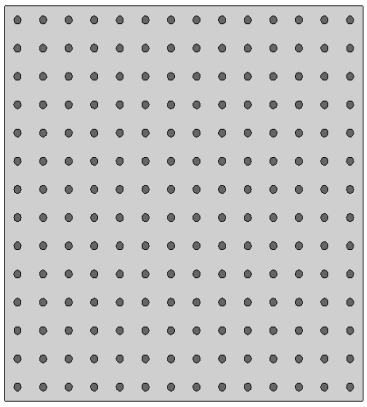

(a) 169 voids resulting in 5.31 % porosity

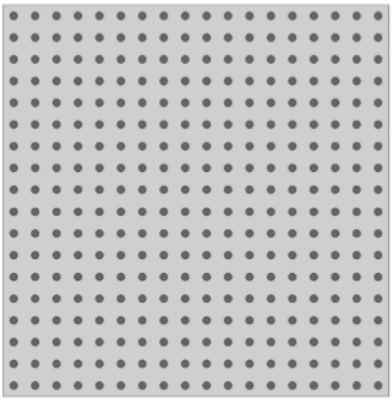

(b) 324 voids resulting in 10.18 % porosity

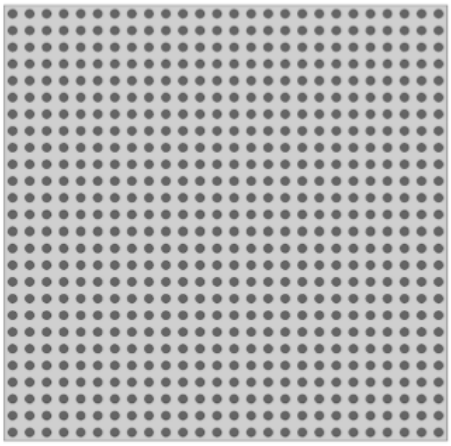

(c) 676 voids resulting in 21.24 % porosity

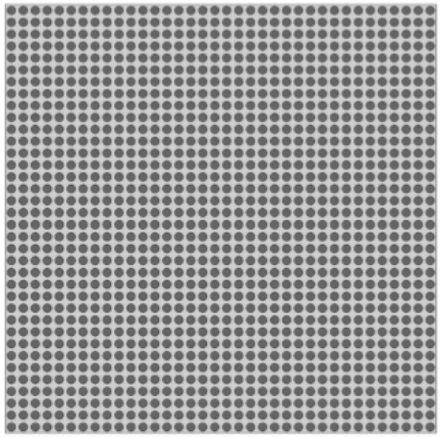

(c) 1296 voids resulting in 40.7 % porosity

Figure 3. Models of porosity simulation.

Table 2. Porosity data.

Model	Parameter	K or A	E_0 or G_0 (MPa)	R^2
Mackenzie	G	K = 2.896	G_0 = 12340.899	0.99872
Mackenzie	E	K = 2.370	E_0 = 29593.245	0.99935
Hanselmann-Hashin	G	A = - 4.976	G_0 = 13148.495	0.97948
Hanselmann-Hashin	E	A = - 3.314	E_0 = 30590.435	0.99187

Preprints (www.preprints.org) | NOT PEER-REVIEWED | Posted: 18 April 2023 doi:10.20944/preprints202304.0521.v1

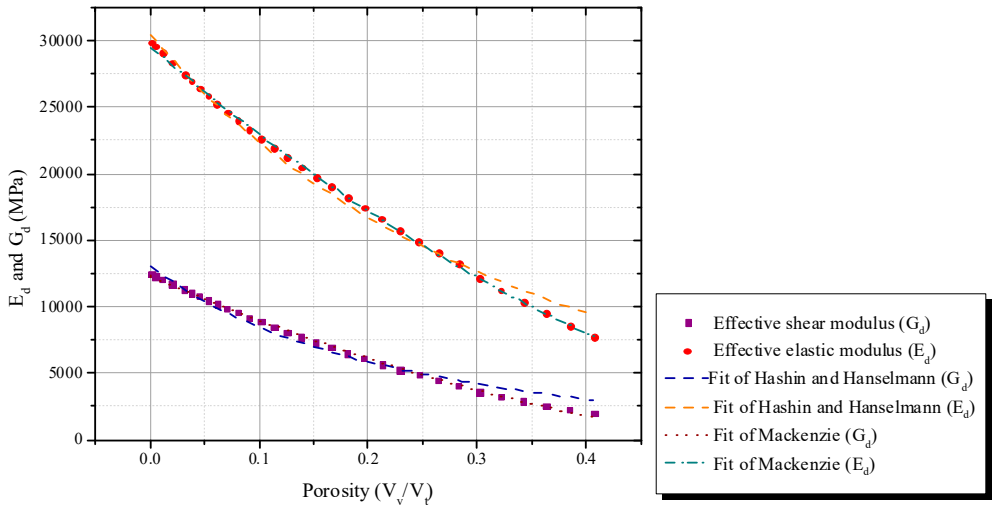

Figure 4. Numerical correlation of E_d or G_d and porosity.

2.3. Biphasic material

A perfectly biphasic material with coarse aggregate (of elastic modulus E_a) perfectly encrusted in a mortar phase (with elastic modulus E_m) without transition zone was simulated and the influence of individual elastic properties of each phase (E_a/E_m), volumetric fraction of the aggregates, and Poisson ratio of each phase on effective E_d was checked. The accuracy of homogenization composite models was measured under the above-mentioned conditions.

2.3.1. Influence of individual elastic properties of phases (E_a/E_m)

We supposed an effective material composed of 625 perfectly spherical aggregates of 4.8 mm diameter, arranged in a mortar, with no transition zone (ITZ) and/or porosity, as shown in Figure 5. An analysis was performed with mortar properties of ρ_m = 2100 kg/m^3, E_m = 10000 MPa, 20000 MPa or 30000 MPa and ν_m = 0.2, and aggregates properties of ρ_a = 2700 kg/m^3, E_a = 30000 MPa, 60000 MPa or 90000 MPa, and ν_a = 0.2.

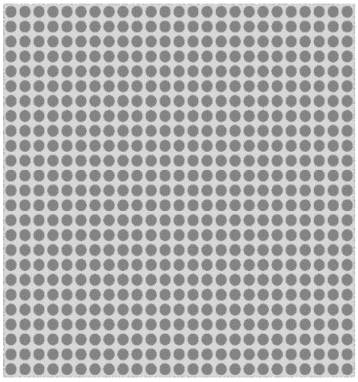

Figure 5. Matrix with encrusted aggregates.

Figure 6 shows an increase in E_a increases E_d in the same volumetric proportion and constant E_m, explained by "Mixture Rule" [9,13]. The gray area in Figure 6 represents ± 5 % error, as of the effective model. This error is used in the verification of the accuracy of classical models and is similar to the admissible error adopted by Duplan et al. [28]. When the elastic modulus of the mortar (E_m = 20000 MPa) and aggregates (E_a = 30000 MPa) were relatively close (i.e., E_a/E_m = 1.5), the prediction of E_d for all classical models was accurate; however, when E_a/E_m > 2, almost all homogenization models

Preprints (www.preprints.org) | NOT PEER-REVIEWED | Posted: 18 April 2023 doi:10.20944/preprints202304.0521.v1

overestimated effective E_d (i.e., Voigt, H-S, Counto, mean of H-S and Voigt-Reuss). An exception of this was Reuss model (series), which underestimated E_d for all cases of E_a/E_m. The Hirsch model calibrated to x = 0.27 accurately represented the phenomenon. The x value is very similar to that obtained experimentally by Topçu for static elastic modulus [11] (i.e., x = 0.3). H-S-Low (and Hansen) also showed a good approximation level, with an almost 5% error. Although, H-S-Low accurately represented the phenomenon, H-S bounds contained no biphasic material. According to Nilsen and Monteiro [16], the H-S limits diverge because concrete is not considered a biphasic material, and a third phase (i.e., transition zone) should be included. This is partially true, since a portion of error due to biphasic H-S does not consider the ITZ phase, nevertheless Figure 6 shows only cases of a perfectly biphasic material with no ITZ. Actually, this divergence of H-S and the biphasic material occur because Hashin-Shtrikman bounds were formulated from a static consideration [18], which is not valid here. Therefore, H-S bounds are not perfectly applied to dynamic situations and should be used with caution for modal analysis. Voigt and Reuss bounds always contain a biphasic material, and a simple average of those limits was inferior to 10 %, when $E_a/E_m < 3$. The same tendency was observed for the H-S average. On the other hand, when E_a extrapolates $E_a/E_m > 3$, Voigt-Reuss and H-S significantly diverge, which causes a very high error.

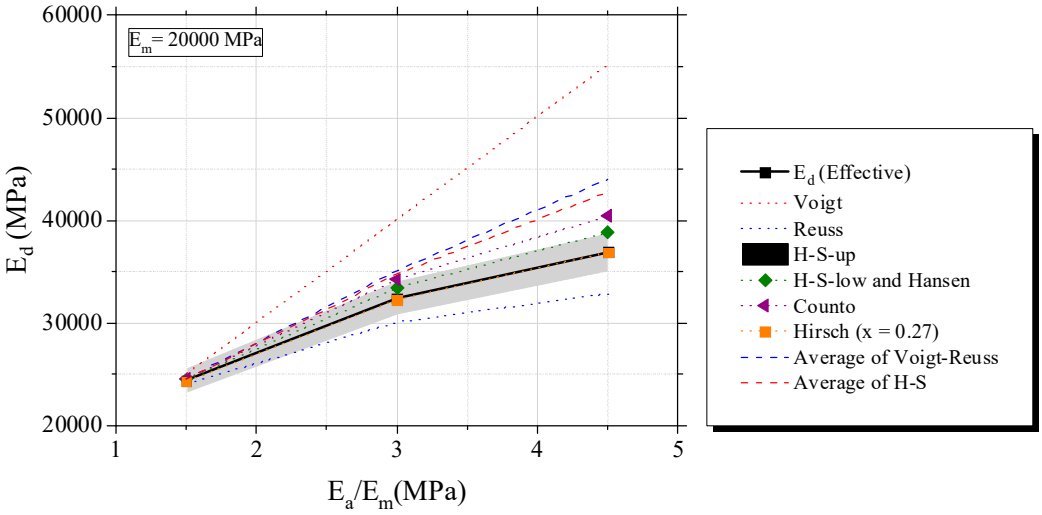

Figure 6. Evaluation of biphasic estimates and Influence of the elastic modulus of the aggregate on effective E_d.

In the same volumetric proportions and E_a, a decrease of E_m (and increase in ration E_a/E_m) decreases E_d, according to Figure 7. About classical biphasic models presented same anteriorly postulated tendencies.

Preprints (www.preprints.org) | NOT PEER-REVIEWED | Posted: 18 April 2023 doi:10.20944/preprints202304.0521.v1

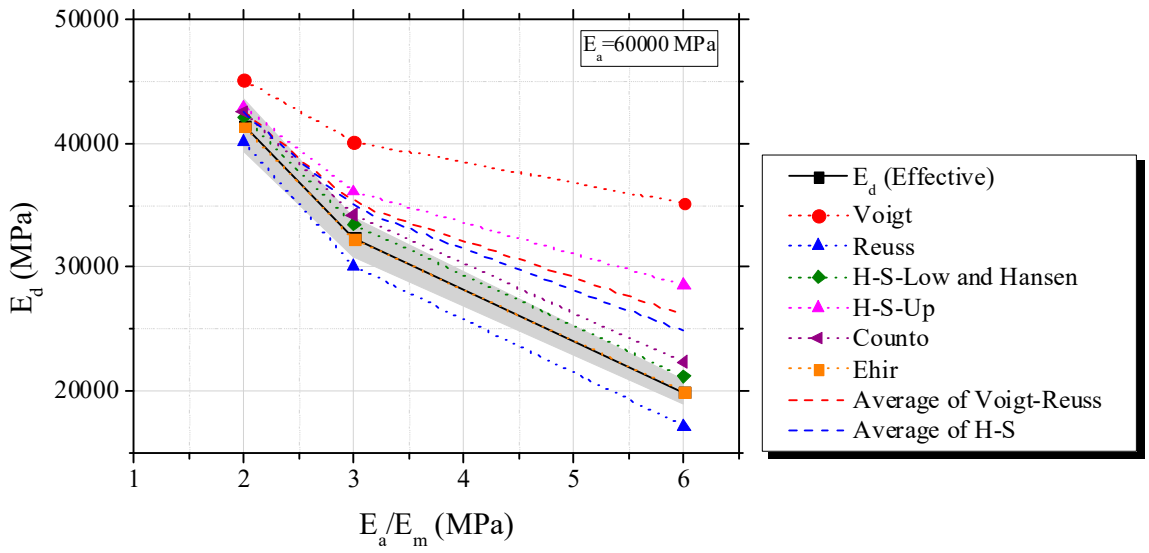

Figure 7. Evaluation of biphasic estimates and Influence of the elastic modulus of the mortar on E_d.

2.3.2. Effect of Volumetric fraction

Variations in the volumetric portion can also influence E_d, with fixed E_a and E_m [1,3,34]. Theoretical materials whose volumetric fraction increases progressively (i.e., 196 to 324 particles, according to Figure 8) were simulated. The aggregate diameter, elastic modulus and density of each phase were constant (ϕ_a = 7.5 mm, E_a = 90000 MPa, E_m = 20000 MPa, ρ_a = 2700 kg/m³ and ρ_m = 2100 kg/m³).

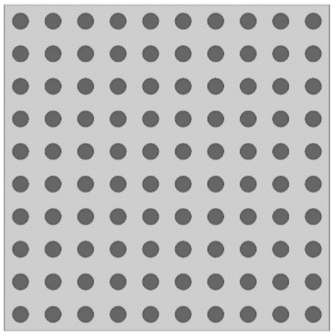

(a) 196 particles - 19.63 % of aggregate

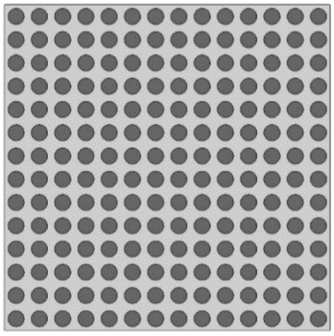

(b) 196 particles - 38.48 % of aggregate

Preprints (www.preprints.org) | NOT PEER-REVIEWED | Posted: 18 April 2023 doi:10.20944/preprints202304.0521.v1

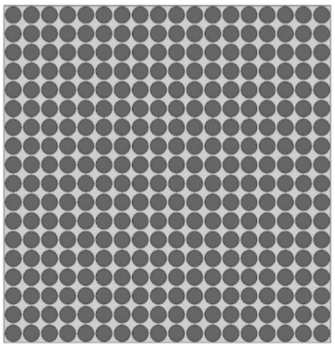

(c) 324 particles - 63.62% of aggregate

Figure 8. Models used in the evaluation of volumetric variation.

Figure 9 shows the correlation between volumetric fraction and E_d. In this case, an H-S and/or Voigt-Reuss average did not describe the phenomenon successfully, since $E_a/E_m > 3$. Hirsch x = 0,27 and H-S-Low accurately captured the phenomenon with 5% error. All tendencies already mentioned are observed.

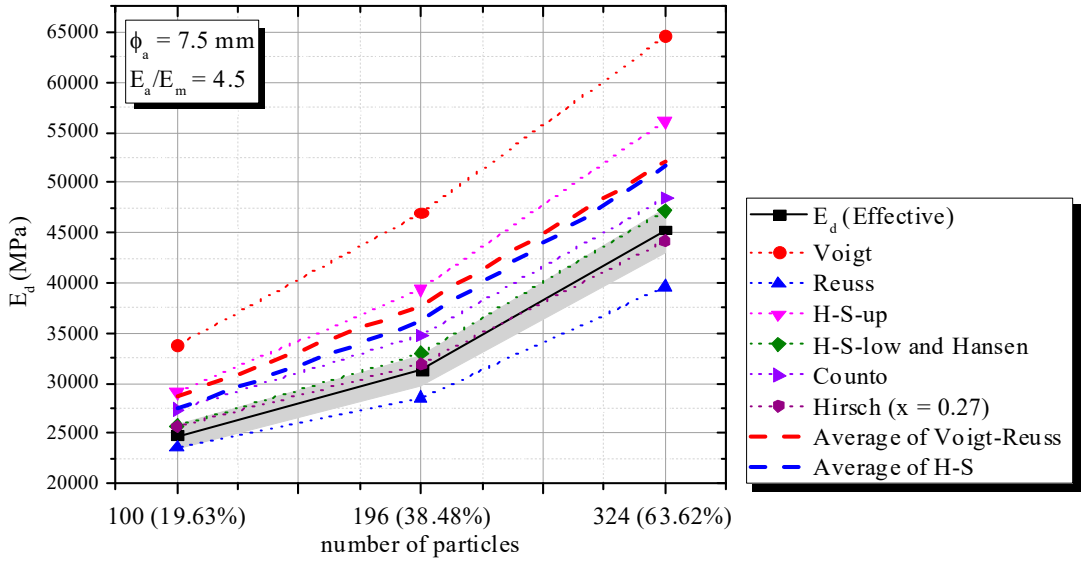

Figure 9. Influence of number of particles and volumetric fraction on E_d.

2.4. Triphasic composite material

The models were constituted by coarse aggregate, mortar and a transition zone with known properties, i.e., 0.05 mm [35,36] - 0.25 mm thickness and $E_m/2$ (E_{ITZ} = 10 GPa) elastic modulus [1,27,35,36]. Two diameters of aggregates, namely ϕ_a = 4.8 mm (256 particles) and ϕ_a = 7.5 mm (625 particles), were used at 50.27% constant volumetric fraction (c_a). For simplicity and reductions in the computational costs, the theoretical material contains no voids.

Figures 14 (ITZ of 0.05 mm), 15 (ITZ of 0.10 mm) and 16 (ITZ of 0.25 mm) show an increase in E_a/E_m increased the composite elastic modulus (E_d), fixed mortar-aggregate proportions and E_m = 20000 MPa. This tendency is very similar to that observed in simulations of a theoretical biphasic material.

According to Figures 14 and 15, Hirsch model with x = 0.27 best predicted E_d for ITZ of 0.05 mm and 0.10 mm, with 5% error. However, it failed to capture the phenomenon when ITZ increased to

Preprints (www.preprints.org) | NOT PEER-REVIEWED | Posted: 18 April 2023 doi:10.20944/preprints202304.0521.v1

0.25 mm and the behavior of the triphasic model was similar to inferior biphasic model, i.e., Reuss (see Figure 16).

Hashin-Shtrikman confirmed again its limitations, i.e., influence of ITZ and application of H-S under dynamic situations. Although H-S bounds showed limitations, H-S-Low revealed good accuracy when ITZ was 0.05 mm (Figure 14) and $E_a/E_m < 3$. A simple average of Voigt-Reuss or H-S showed errors higher than 5 %.

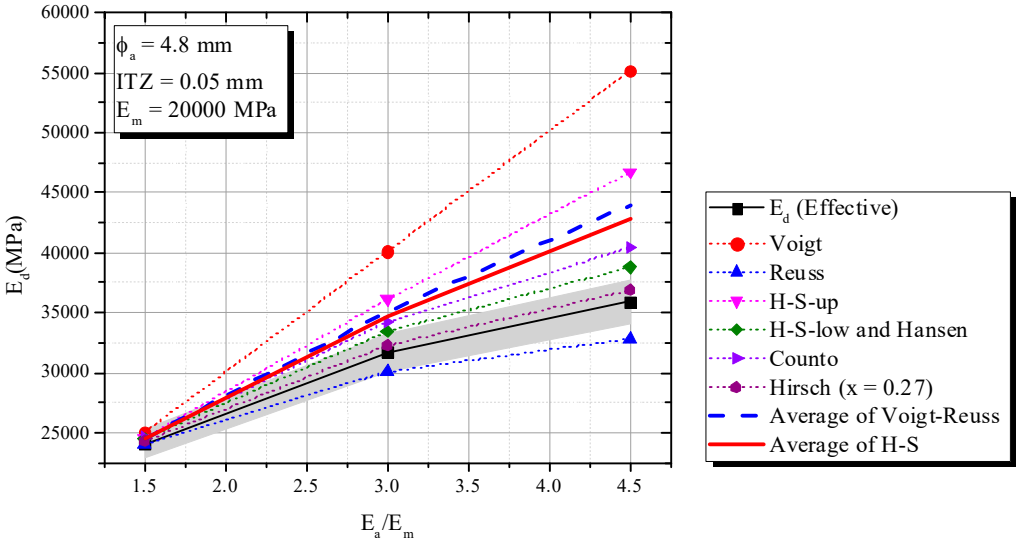

(a) ϕ_a = 4.8 mm and ITZ = 0.05 mm

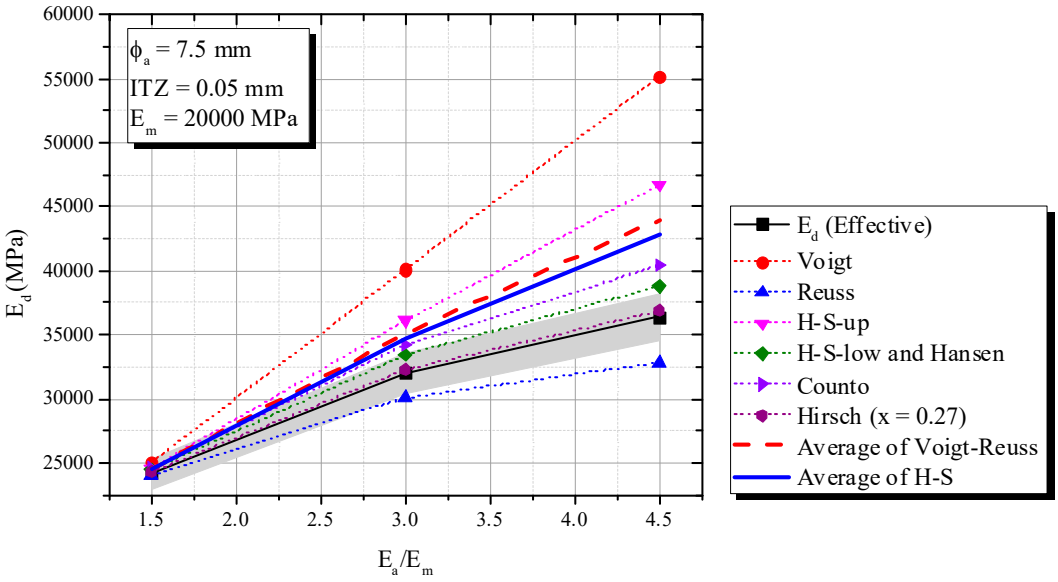

b) ϕ_a = 7.5 mm and ITZ = 0.05 mm

Figure 14. Influence of E_a/E_m (triphasic composite with ITZ = 0.05 mm) on E_d in comparison with biphasic models.

Preprints (www.preprints.org) | NOT PEER-REVIEWED | Posted: 18 April 2023 doi:10.20944/preprints202304.0521.v1

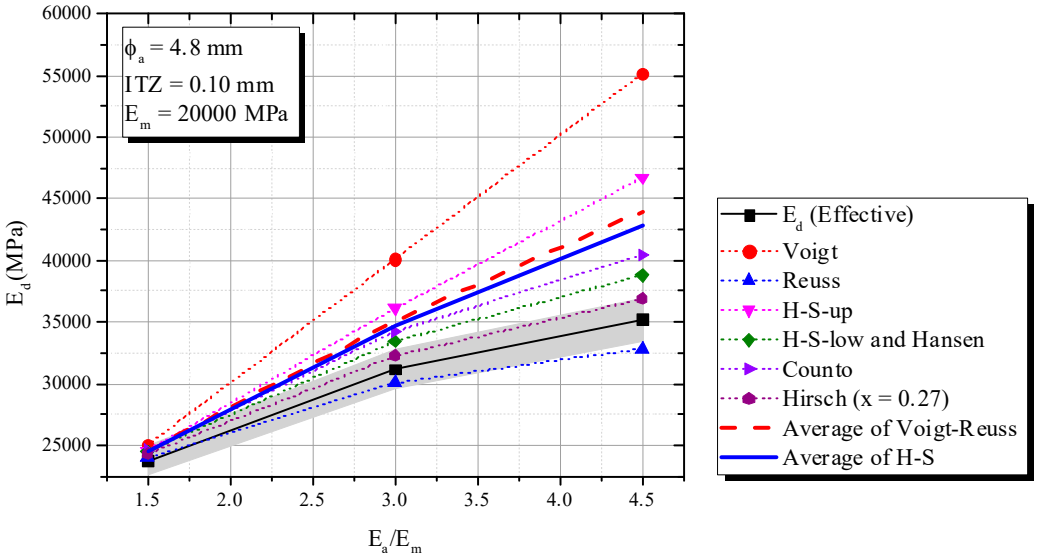

(a) ϕ_a = 4.8 mm and ITZ = 0.10 mm

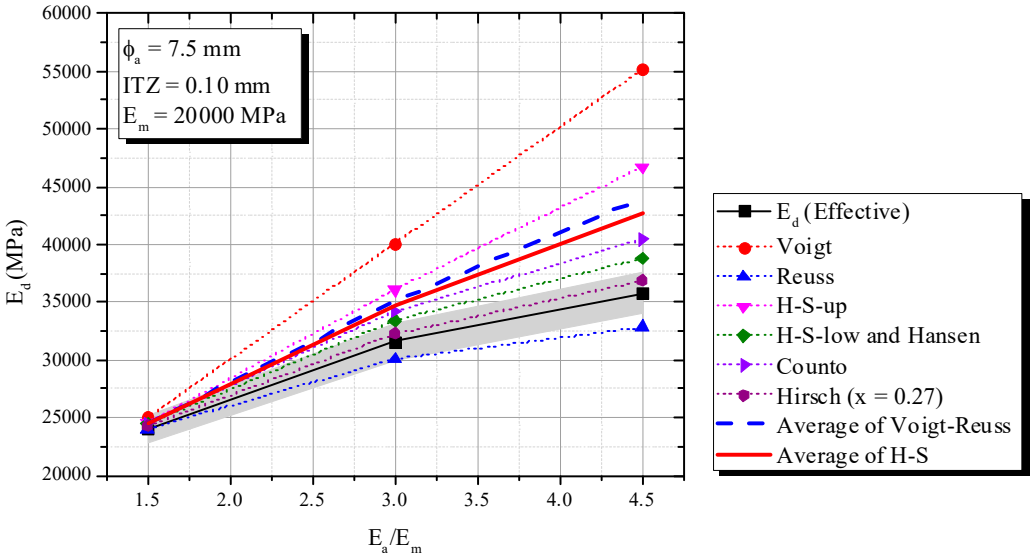

(b) ϕ_a = 7.5 mm and ITZ = 0.10 mm

Figure 15. Influence of E_a/E_m (triphasic composite with ITZ = 0.10 mm) on E_d in comparison with biphasic models.

Preprints (www.preprints.org) | NOT PEER-REVIEWED | Posted: 18 April 2023 doi:10.20944/preprints202304.0521.v1

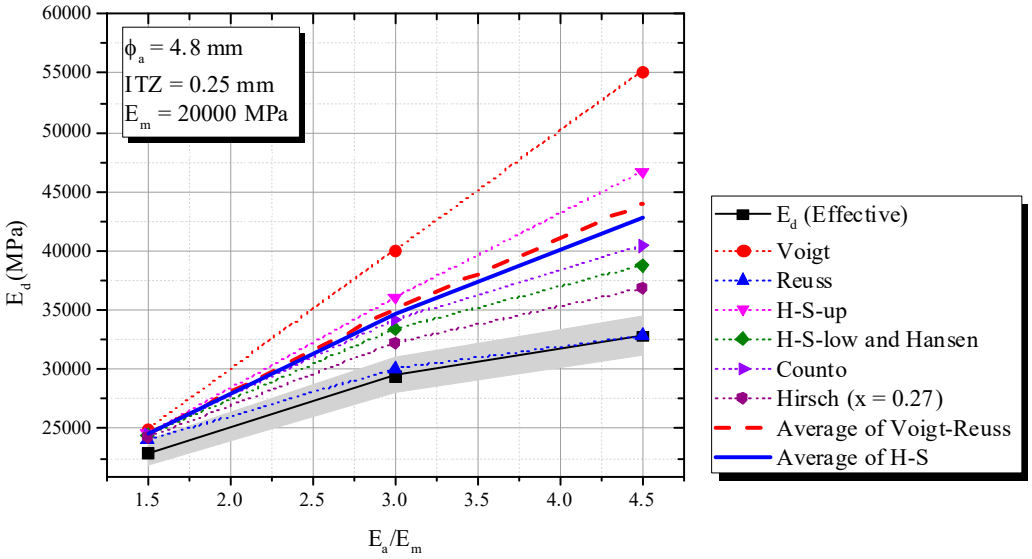

(a) ϕ_a = 4.8 mm and ITZ = 0.25 mm

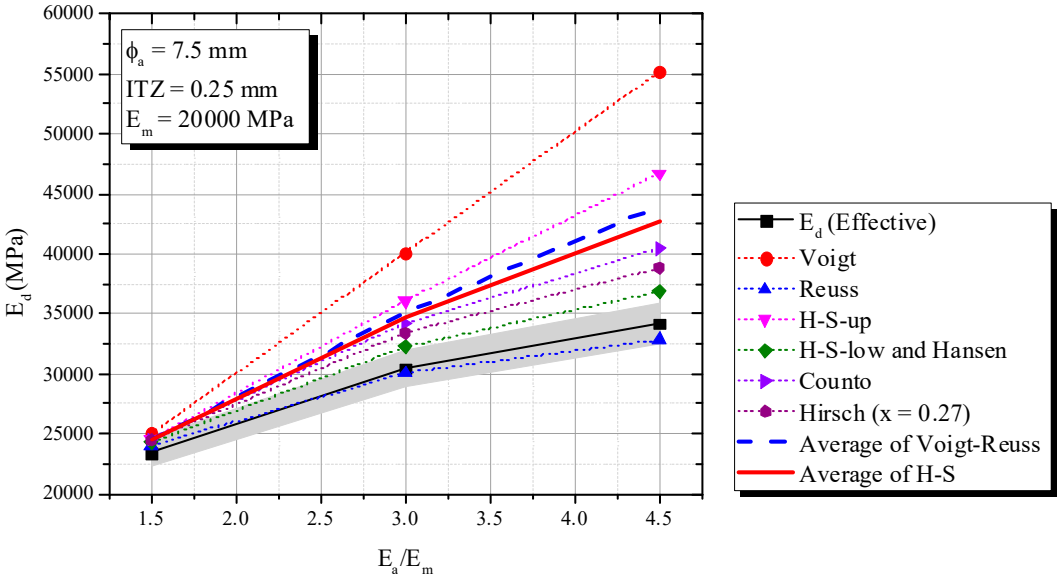

(b) ϕ_a = 7.5 mm and ITZ = 0.25 mm

Figure 16. Influence of E_a/E_m (triphasic composite with ITZ = 0.25 mm) on E_d in comparison with biphasic models.

Classic biphasic models can consider ITZ, if applied twice, for the obtaining of a triphasic material. The methodology consists in the obtaining of a preliminary composite constituted by mortar and ITZ and associated with a coarse aggregate for the generation of a triphasic composite. Figure 17 shows the numerical data for ϕ_a = 4.5 mm, E_a/E_m = 4.5 or 3, E_m = 20000 MPa and variable ITZ. Although ITZ is incorporated, the same tendencies above mentioned are observed.

Preprints (www.preprints.org) | NOT PEER-REVIEWED | Posted: 18 April 2023 doi:10.20944/preprints202304.0521.v1

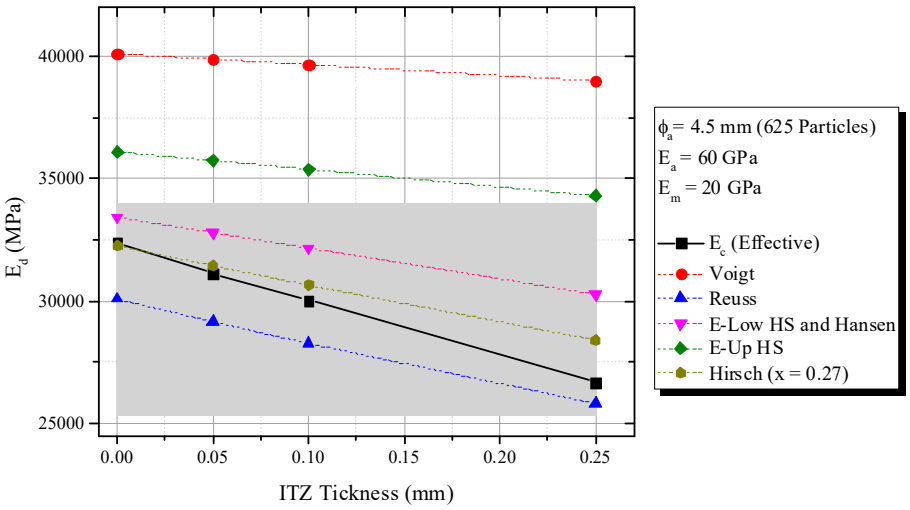

(a) ϕ_a = 4.5 mm, E_a/E_m = 3 and variable ITZ

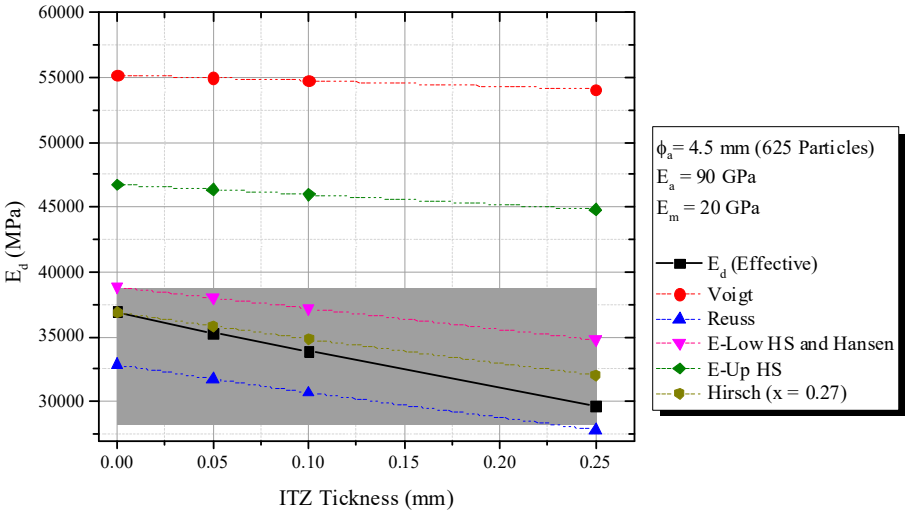

(b) ϕ_a = 4.5 mm, E_a/E_m = 4.5 and variable ITZ

Figure 17. Triphasic model prediction and influence of ITZ thickness.

3. Experimental validation

3.1. Materials and mixes

Concrete and mortar samples were produced for the validation of the numerical study. Portland cement type III of 3.10 g/cm³ density, specified according to the classification of ASTM C150 [37] and ABNT NBR 5733:1991[38], was used in the samples. Natural sand of 2.19 fineness modulus [39] and 2.65 g/cm³ density and crushed diabase of 3.30 g/cm³ density and 12.5 mm nominal maximum sizes were used as aggregates. Their grading curves are shown in Figure 18.

Preprints (www.preprints.org) | NOT PEER-REVIEWED | Posted: 18 April 2023 doi:10.20944/preprints202304.0521.v1

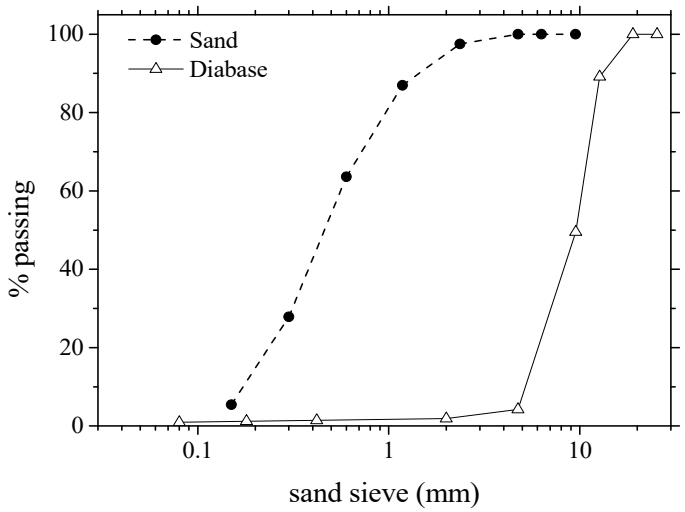

Figure 18. Grading curves of aggregates.

The proportions (in weight) of mortar and concrete mixtures are shown in Tables 5.a and 5.b. Water cement ratios, amounts of sand, coarse aggregates and superplasticizers were varied among the mixtures. The production of mortars and/or concrete samples consisted in (i) mix the cement and aggregates with no water addition, then (ii) water was a then added and the mixing procedure was performed until the material had shown a homogeneous appearance. After hardening, the molds were removed and immediately stored in a moist chamber for curing until the age of testing.

Table 5.a. Unitary mix proportions of mortars.

ID	cement (kg)	sand (kg)	water (kg)	superplasticizer (kg)
1-M	1.00	2.00	0.50	0.010 (1%)
2-M	1.00	2.00	0.30	0.010 (1%)
3-M	1.00	2.00	0.70	0

Table 5.b. Unitary mix proportions of concretes.

ID	Cement (kg)	Sand (kg)	Coarse Aggregate (kg)	water (kg)	superplasticizer (kg)
1-C	1.00	2.00	3.00	0.50	0.010 (1%)
2-C	1.00	2.00	3.00	0.30	0.010 (1%)
3-C	1.00	2.00	3.00	0.70	0

3.2. Specimens

The following samples were produced:

(i) Mortars (1-M, 2-M and 3-M) - five prismatic specimens of 40 mm x 40 mm x 160 mm).
(ii) Concretes (1-C, 2-C and 3-C) - five prismatic specimens of 150 mm x 150 mm x 500 mm.
(iii) Rocks' samples - Five cylindrical samples of 55 mm x 125 mm made by core drills extracted from an intact diabase rock.

3.3. Acoustic tests and evaluation of experimental E_d

Acoustic tests (Figure 19.a) were performed in mortars and concretes specimens, according to ASTM C215 [4]. The mass of each sample was measured prior to each acoustic test. The sample was

Preprints (www.preprints.org) | NOT PEER-REVIEWED | Posted: 18 April 2023 doi:10.20944/preprints202304.0521.v1

then positioned on steel wires attached to a metal frame (Figure 19.a) and an impact was manually applied with a hammer on the surface of the specimen, while a microphone captured the sound radiated by the specimen's surface in another position. Depending on the vibration mode evaluated (flexural, torsional or longitudinal), different impact and measurement positions were selected, as suggested by ASTM E1876-01 [5] and shown schematically in Figure 20. The first two modes of each type (flexural, torsional and longitudinal) (see Figure 21) were easily identified in the prismatic specimens. However, this study focused on 1st flexural and 1st longitudinal modes (see Figures 19.c and 21), i.e., the necessary vibration modes for the obtaining of the dynamic elastic modulus (E_d). After excitation, an onboard sound card of a regular notebook captured the acoustic signal at a 96 kHz acquisition rate. Figure 19.b shows a typical time vs. amplitude signal in a prismatic concrete sample tested at 28 days of age, obtained by an impact applied for activating the flexural and longitudinal modes (eccentric excitation). The first 1024-point block was selected, multiplied by a Hanning window and then zero-padded for the obtaining of an 8192-point vector. A Fast Fourier Transform was applied for the detection of peaks of natural frequencies.

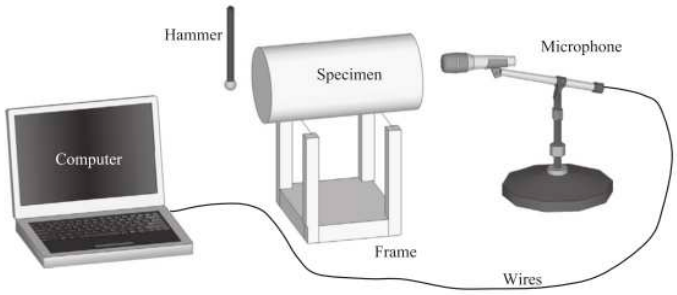

(a) Scheme of Acoustic Test

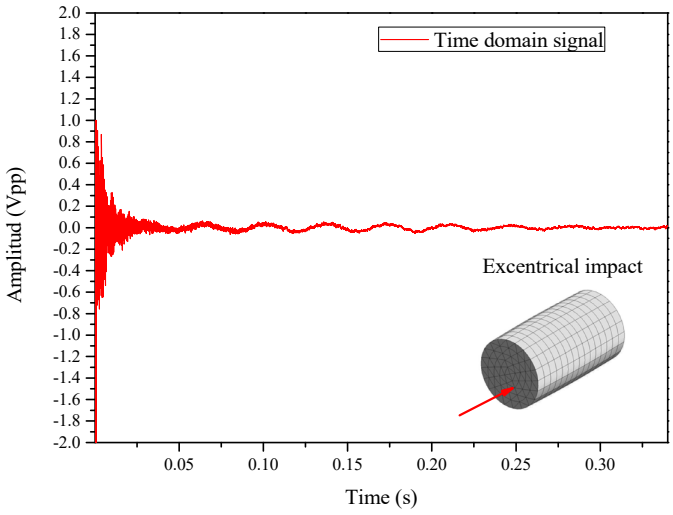

(b) Time domain

Preprints (www.preprints.org) | NOT PEER-REVIEWED | Posted: 18 April 2023 doi:10.20944/preprints202304.0521.v1

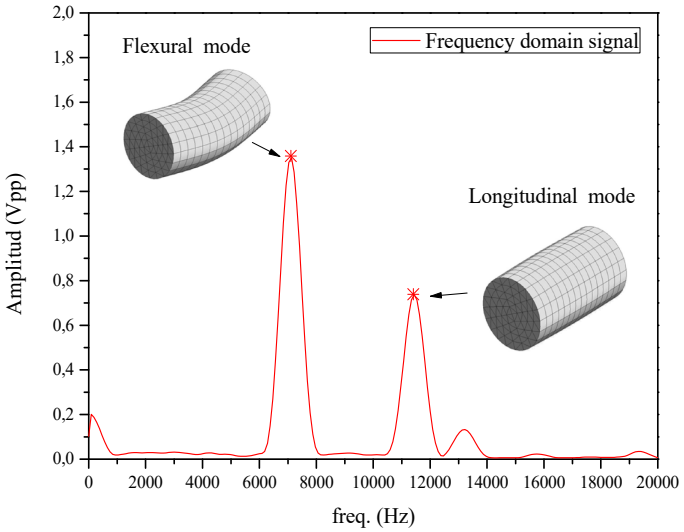

(c) Frequency domain

Figure 19. (a) Scheme of acoustic test; (b) Time domain and (c) Frequency domain.

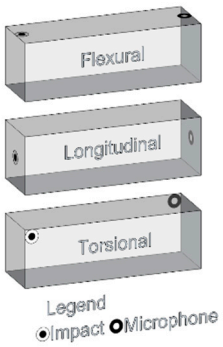

Figure 20. Excitation and measurement positions for the different vibration modes investigated.

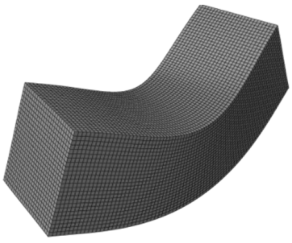

First flexural mode (1F)

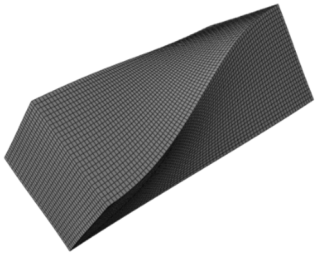

First torsional mode (1T)

Preprints (www.preprints.org) | NOT PEER-REVIEWED | Posted: 18 April 2023 doi:10.20944/preprints202304.0521.v1

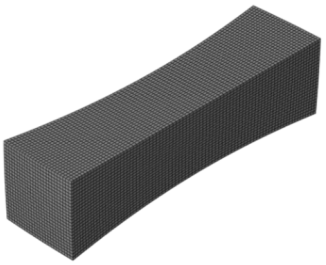

First longitudinal mode (1L)

Figure 21. Fundamental vibration modes investigated.

Once experimental $f_{1,flex}$ and $f_{1,long}$ are obtained by acoustic test and exciting flexural and/or longitudinal vibrations modes, the elastic properties are evaluated through frequency equations, according to ASTM E1876 [5]. The sample's dynamic modulus of elasticity (E_d) was obtained from the first flexural mode of vibration ($E_{d,f}$) by Eqs. 6 and 7, for prismatic or cylindrical specimens, respectively:

$$E_{d,f} = 0.9465 \frac{mL^3}{bt^3} f_{flex,1}{}^2 B \quad (6)$$

$$E_{d,f} = 1.6067 \frac{mL^3}{D^4} f_f{}^2 A \quad (7)$$

where b and t are dimensions of the prismatic cross section, D is the diameter of the cylindrical cross section, L is the specimen length, m is the specimen mass (in kg) and A and B are a correction factor dependent on Poisson coefficient (ν, generally 0.20, according to Mehta and Monteiro [1]) and dimensions of the specimens (b, t and D), computed by Eqs. 8 and 9:

$$A = 1 + 4.939(1 + 0.0752\upsilon_d + 0.8109\upsilon_d{}^2)\left(\frac{D}{L}\right)^2 - 0.4883\left(\frac{D}{L}\right)^4 - \left[\frac{4.691\left(1 + 0.2023\upsilon_d + 2.173\upsilon_d{}^2\right)\left(\frac{D}{L}\right)^4}{1.000 + 4.754\left(1 + 0.1408\upsilon_d + 1.536\upsilon_d{}^2\right)\left(\frac{D}{L}\right)^2}\right] \quad (8)$$

$$B = 1 + 6.585(1 + 0.0752\upsilon_d + 0.8109\upsilon_d{}^2)\left(\frac{t}{L}\right)^2 - 0.868\left(\frac{t}{L}\right)^4 - \left[\frac{8.340\left(1 + 0.2023\upsilon_d + 2.173\upsilon_d{}^2\right)\left(\frac{t}{L}\right)^4}{1.000 + 6.338\left(1 + 0.1408\upsilon_d + 1.536\upsilon_d{}^2\right)\left(\frac{t}{L}\right)^2}\right] \quad (9)$$

Similarly, the dynamic modulus of elasticity was obtained from the first longitudinal mode of vibration ($E_{d,l}$), in accordance with Eq. 10 for prismatic specimens:

$$E_{d,l} = 4 \frac{mL}{bt} f_l^2 \frac{1}{K} \quad (10)$$

In this case, K is a correction factor given by Eq. 11 and D_e is the effective diameter of the bar, equal to D for a cylinder and given by Eq. 12 for a prismatic specimen.

$$K = 1 - \frac{\pi^2 \nu_d{}^2 D_e{}^2}{8L^2} \quad (11)$$

$$D_e{}^2 = 2\frac{b^2 + t^2}{3} \quad (12)$$

Preprints (www.preprints.org) | NOT PEER-REVIEWED | Posted: 18 April 2023 doi:10.20944/preprints202304.0521.v1

3.4. Experimental Results and discussion

The problem of evolution of elastic modulus over time was chosen to demonstrate the observed tendencies presented in above numerical results. All curves were calibrated by CEB FIB [40] (Eq. 13 and 14) for ages of 1 to 60.

$$E(t) = \beta_E \times E_{28} (13)$$

where E (t) is the function that represents the evolution of the elastic modulus over time, E28 is the modulus of elasticity at 28 days, and β_E is the contribution of time, according to Eq. 14:

$$\beta_E = \left\{ \exp\left\{ s\left[1 - \left(\frac{28}{t} \right)^{0,5} \right] \right\} \right\}^{0,5} \quad (14)$$

The input of the biphasic model was the evolution over time of the dynamic elastic modulus of mortar E_m (see Figure 22.a) and the dynamic elastic modulus of samples of diabase rock E_a (see Figure 22.b).

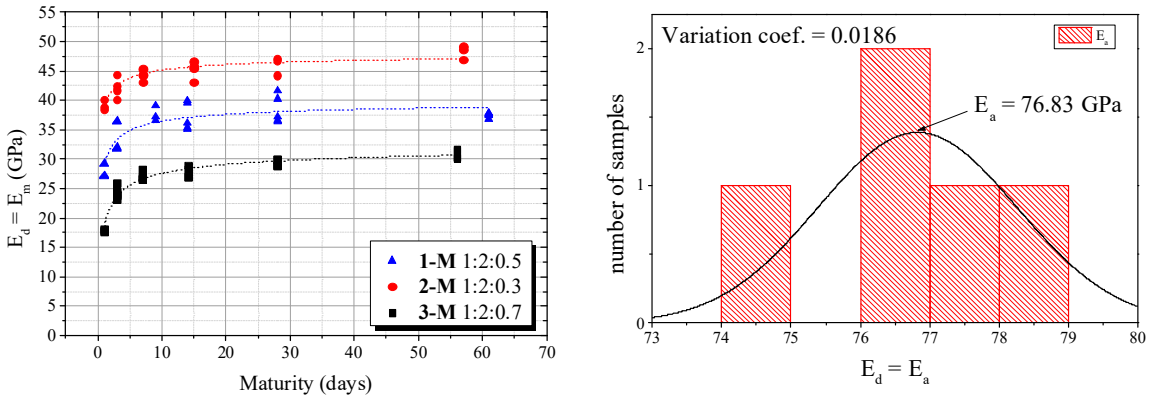

(a) (b)

Figure 22. E_d for (a) mortars and (b) diabasic rock.

Figures 23.a, b and c show the behavior of the dynamic elastic modulus of the concrete (E_d) over time and the biphasic models that predicted this evolution.

Preprints (www.preprints.org) | NOT PEER-REVIEWED | Posted: 18 April 2023 doi:10.20944/preprints202304.0521.v1

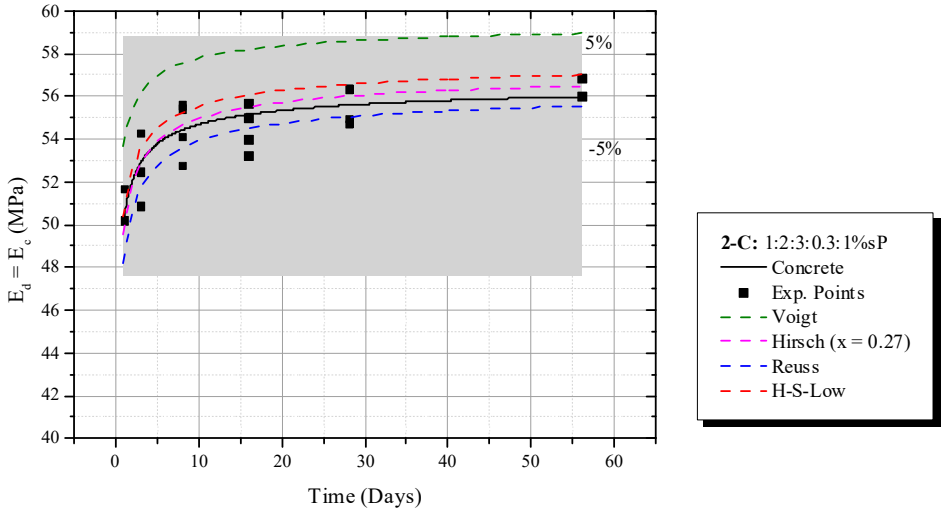

(a)

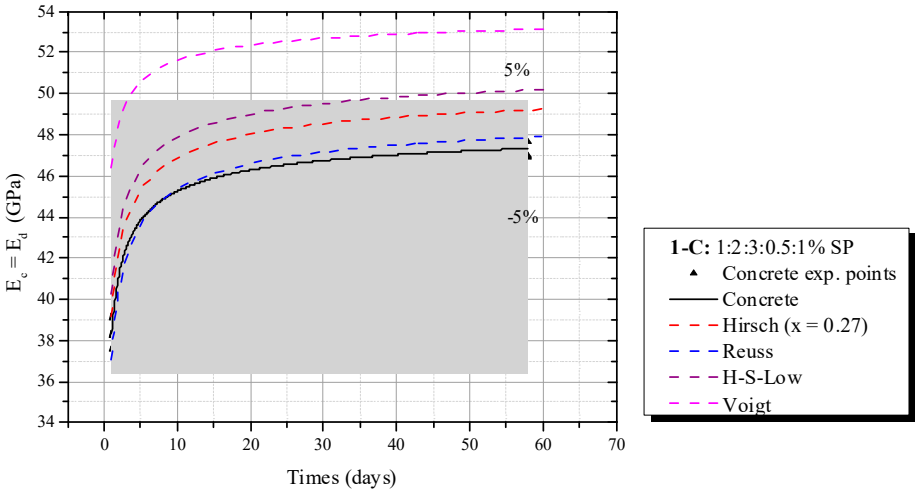

(b)

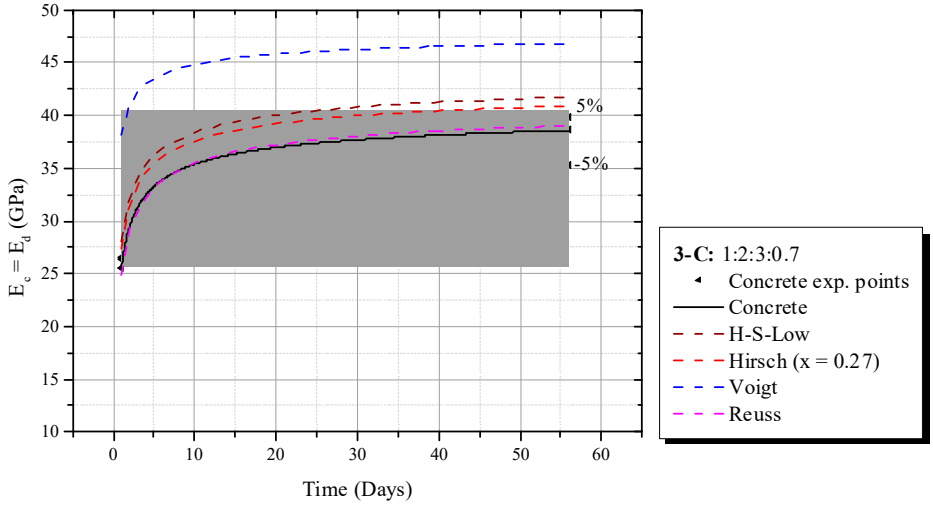

(c)

Figure 23. Evolution of E_d for w/c = (a) 0.3 , (b) 0.5 and (c) 0.7.

The experimental investigation showed Hirsch (x = 0.27) achieved good accuracy when w/c = 0.3 and 0.5, with errors within the 5% limit and identical to the maximum error observed in numeric simulations. However, its absolute error was slightly higher than 5 % for concretes with w/c = 0.7. This phenomenon is explained by a complex interaction of mortar, ITZ, water and coarse aggregate surface at early ages. According to Simeonov and Ahmad [17], a fresh concrete mixture undergoes a process of water migration to the surface of the coarse aggregates and this "water attraction" increase the ITZ thickness. Such a decrease is more pronounced at high water-cement ratios (e.g. w/c = 0.7), the $E_d(t)$ curve moves to Reuss model, which also justified the same tendency of concretes with w/c = 0.5 (within 5% error). Therefore, numerical simulations revealed that, when ITZ increases, the best prediction is achieved by Reuss model, similarly to the experimental behavior. On the other hand, this phenomenon is reduced for concretes with little ITZ (e.g. w/c = 0.3) and dynamic elastic modulus is very close to Hirsch (x = 0.27).

4. Conclusions and final remarks

Numerical simulations of a porous, biphasic and triphasic material were developed. The study was focused in dynamic elastic modulus. The main finds are:

(i) Homogenization composite models as Reuss and Hirsch (x = 0.27) are simple and accuracy ways to predict the dynamic elastic modulus with 5 % maximum error, regarding the ITZ conditions. Hirsch (x = 0.27) best predicts E_d for ITZ = 0.05 mm and 0.10 mm while Reuss model for ITZ = 0.25 mm. In the experimental field, a similar tendency was observed, once Hirsch (x = 0.27) successfully represented the E_d (t) phenomenon for concretes with low and moderate water cement ratios (w/c = 0.3 and 0.5), and Reuss was the only to predict the mixture with w/c = 0.70 with an error always lower than 5%;

(ii) Voigt, H-S and Hansen always overestimate E_d for all numerical simulations and experimental validation;

(iii) Hashin-Shtrikman limits does not contain biphasic theoretical models and cannot be applied to dynamic situations perfectly [18];

(iv) Although biphasic models, as Reuss, Hirsch (x = 0.27), Voigt and H-S have incorporated ITZ, they will display the same tendencies observed for classic biphasic models. An advantage is the predict of the decrease in E_d in function of ITZ.

(v) The effective Poisson ratio obtained by natural frequency shows a considerable error, due to some degree of anisotropy generated by the configuration of aggregates inside the mortar. The arrangement of coarse aggregates also influences this measure, since different arrangements with same elastic properties and volumetric fraction might generate a certain divergency in the Poisson ratio.

Our study has enhanced our understanding of the response of concrete under dynamical excitations. Numerical simulations of the theoretical material enabled the refining of the models, hence, a reliable and prudent control of dynamic deflections and verification of natural frequencies of the concrete's structures.

References

1. P.J.M. Mehta, P.K.; Monteiro, Concreto: Estrutura, Propriedades e Materiais, 3a, McGraw-Hil, New York, 2008.
2. V.M. Malhotra, V. Sivasundaram, Resonant Frequency Methods * 7.1 7.2, in: Nondestruct. Test. Concr., 1st ed., CRC PRESS, New York, 1989.
3. A.M. Neville, Propriedades Do Concreto, 2a, PINI, São Paulo, 1997.
4. American Society for Testing and Materials ASTM C215-02, Standard Test Method for Fundamental Transverse , Longitudinal, and Torsional Resonant Frequencies of Concrete Specimens, in: 2003: pp. 1–7.

5. American Society for Testing and Materials ASTM E1876-01, Standard Test Method for Dynamic Young ' s Modulus , Shear Modulus , and Poisson ' s Ratio by Impulse Excitation of Vibration, (2001).
6. N. Swamy, G. Rigby, Dynamic properties of hardened paste , mortar and concrete, Matériaux Constr. (1971) 13–40.
7. N.S. Bawa, J.W.S. Graft-Johnson, Effect of Mix Proportion , Water-Cement Ratio , Age and Curing Conditions on the Dynamic Modulus of Elasticity of Concrete, Build. Sci. 3 (1969) 171–177.
8. F.D. Lydon, M. Iacovou, SOME FACTORS AFFECTING THE DYNAMIC MODULUS OF ELASTICITY OF HIGH STRENGTH CONCRETE, Cem. Concr. Res. 25 (1995) 1246–1256.
9. W. Voigt, Úber die Beziehung zwischen den beiden Elastizi ä tskonstanten isotroper Körper, Wied. Ann. J. 38 (1889) 573–587.
10. P.J.M. Monteiro, C.T. Chang, The elastic moduli of calcium hydroxide, Cem. Concr. Res. 25 (1995) 1605–1609. doi:10.1016/0008-8846(95)00154-9.
11. İ.B. Topçu, Alternative estimation of the modulus of elasticity for dam concrete, Cem. Concr. Res. 35 (2005) 2199–2202. doi:10.1016/j.cemconres.2004.08.010.
12. İ.B. Topçu, T. Bilir, A.R. Boğa, Estimation of the modulus of elasticity of slag concrete by using composite material models, Constr. Build. Mater. 24 (2010) 741–748. doi:10.1016/j.conbuildmat.2009.10.034.
13. A. Reuss, Berchung der Fiessgrenze von Mischkristallen auf Grund der Plastizi ä tsbedingung für Einkristalle, Zeitschrift Für Angew. Math. Und Mech. 9 (1929) 49–58. doi:10.1002.
14. R. Hill, The Elastic Behaviour of a Crystalline Aggregate, Proc. Phys. Soc. 65 (1952) 349–354.
15. Z. Hashin, S. Shtrikman, A VARIATIONAL APPROACH TO THE THEORY OF THE ELASTIC BEHAVIOUR OF MULTIPHASE MATERIALS, J. Mech. Phys. Solids. 11 (1963) 127–140.
16. U. Nilsen, P.J.M. Monteiro, CONCRETE: A THREE PHASE MATERIAL, Cem. Concr. Res. 23 (1993) 147–151.
17. P. Simeonov, S. Ahmad, Effect of transition zone on the elastic behavior of cement-based composites, Cem. Concr. Res. 25 (1995) 165–176. doi:10.1016/0008-8846(94)00124-H.
18. S. Nemat-nasser, A. Srivastava, Journal of the Mechanics and Physics of Solids Bounds on effective dynamic properties of elastic composites, J. Mech. Phys. Solids. 61 (2013) 254–264. doi:10.1016/j.jmps.2012.07.003.
19. E.J. Garboczi, J.G. Berryman, Elastic moduli of a material containing composite inclusions: effective medium theory and finite element computations, Mech. Mater. 33 (2001) 455–470. doi:10.1016/S0167-6636(01)00067-9.
20. G. Constantinides, F.J. Ulm, The effect of two types of C-S-H on the elasticity of cement-based materials: Results from nanoindentation and micromechanical modeling, Cem. Concr. Res. 34 (2004) 67–80. doi:10.1016/S0008-8846(03)00230-8.
21. Q. Chen, M.M. Nezhad, Q. Fisher, H.H. Zhu, Multi-scale approach for modeling the transversely isotropic elastic properties of shale considering multi-inclusions and interfacial transition zone, Int. J. Rock Mech. Min. Sci. 84 (2016) 95–104. doi:10.1016/j.ijrmms.2016.02.007.
22. J. Zheng, X. Zhou, L. Sun, Analytical solution for Young's modulus of concrete with aggregate aspect ratio effect, Mag. Concr. Res. 67 (2015) 963–971. doi:10.1680/macr.14.00245.
23. J.J. Zheng, Y.F. Wu, X.Z. Zhou, Z.M. Wu, X.Y. Jin, Prediction of young's modulus of concrete with two types of elliptical aggregate, ACI Mater. J. 111 (2014) 603–612. doi:10.14359/51687232.
24. J. Zheng, X. Zhou, X. Jin, An n-layered spherical inclusion model for predicting the elastic moduli of concrete with inhomogeneous ITZ, Cem. Concr. Compos. 34 (2012) 716–723. doi:10.1016/j.cemconcomp.2012.01.011.
25. Kamtornkiat Musiket; Mitchell Rosendahl; and Yunping Xi, Fracture of Recycled Aggregate Concrete under High Loading Rates, J. Mater. Civ. Eng. 25 (2016) 864–870. doi:10.1061/(ASCE)MT.1943-5533.
26. B. Pichler, C. Hellmich, J. Eberhardsteiner, Spherical and acicular representation of hydrates in a micromechanical model for cement paste: Prediction of early-age elasticity and strength, Acta Mech. 203 (2009) 137–162. doi:10.1007/s00707-008-0007-9.
27. Hashin;, P.J.M. Monteiro, A Novel Approach to Determine the Elastic Properties of the Interphase between the Aggregate and the Cement Paste, Key Eng. Mater. 462–463 (2011) 680–685. doi:10.4028/www.scientific.net/KEM.462-463.680.
28. F. Duplan, A. Abou-Chakra, A. Turatsinze, G. Escadeillas, S. Brule, F. Masse, Prediction of modulus of elasticity based on micromechanics theory and application to low-strength mortars, Constr. Build. Mater. 50 (2014) 437–447. doi:10.1016/j.conbuildmat.2013.09.051.

29. G. Pickett, Equations for Computing Elastic Constants from Flexural and Torsional Resonant Frequencies of Vibration of Prisms and Cylinders, Proc. Am. Soc. Test. Mater. 45 (1945) 846–866.
30. A.R. Boccaccini, Z. Fan, A new approach for the young's modulus-porosity correlation of ceramic materials, Ceram. Int. 23 (1997) 239–245. doi:10.1016/S0272-8842(96)00033-8.
31. D.P.H. HASSELMAN, On the Porosity Dependence of the Elastic Moduli of Polycrystalline Refractory Materials, J. Am. Ceram. Soc. 45 (1962) 452–453. doi:10.1111/j.1151-2916.1962.tb11191.x.
32. Z. Hashin, The Elastic Moduli of Heterogeneous Materials, J. Appl. Mech. 29 (1962) 143. doi:10.1115/1.3636446.
33. J.K. Mackenzie, No Title, Proc. Phys. Soc. 63B (1950) 2–11.
34. Shehata, Deformações Instantâneas do Concreto, in: G.C. Isaia (Ed.), Concreto, Ensino, Pesqui. e Realiz., Ibracon, São Paulo, 2005: pp. 631–685.
35. Z. Jia, Y. Han, Y. Zhang, C. Qiu, C. Hu, Z. Li, Quantitative characterization and elastic properties of interfacial transition zone around coarse aggregate in concrete, J. Wuhan Univ. Technol. Sci. Ed. 32 (2017) 838–844. doi:10.1007/s11595-017-1677-8.
36. G. Li, Y. Zhao, S.-S. Pang, Y. Li, Effective Young's modulus estimation of concrete, Cem. Concr. Res. 29 (1999) 1455–1462. doi:10.1016/S0008-8846(99)00119-2.
37. American Society for Testing and Materials - standard specification for Portland cement, (2011).
38. Associação Brasileira de Normas Técnicas, ABNT NBR 5733 - Cimento Portland de alta resistência inicial, (1991) 1–5.
39. Associação Brasileira de Normas Técnicas. ABNT, ABNT NBR 7211 - Agregados para concreto - Especificação, in: 2009.
40. CEB FIB - COMITÉ EURO-INTERNACIONAL DU BÉTON, Model Code 2010, (2010).